Research Article Vol. 29, No. 11 / 24 May 2021 / Optics Express 16153
Optics EXPRESS

Experimental determination of nanocomposite grating structures by light- and neutron-diffraction in the multi-wave-coupling regime

MARTIN FALLY,[1] YASUO TOMITA,[2] ANTONIO FIMIA,[3] ROQUE F. MADRIGAL,[3] JINXIN GUO,[2,5] JOACHIM KOHLBRECHER,[4] AND JÜRGEN KLEPP[1,*]

[1] *Faculty of Physics, University of Vienna, 1090 Vienna, Austria*
[2] *Department of Engineering Science, University of Electro-Communications, 1-5-1 Chofugaoka, Chofu, Tokyo 182, Japan*
[3] *Department of Material Science, Optics and Electronic Technology, University Miguel Hernández, Elche, Alicante, Spain*
[4] *Laboratory for Neutron Scattering, ETH Zurich & Paul Scherrer Institut, 5232 Villigen PSI, Switzerland*
[5] *Present address: Institute of Information Photonics Technology, Faculty of Science, Beijing University of Technology, Beijing 100124, China*
[*] *juergen.klepp@univie.ac.at*

Abstract: We experimentally demonstrate how to accurately retrieve the refractive index profile of photonic structures by standard diffraction experiments and use of the rigorous coupled-wave analysis in the multi-wave coupling regime, without the need for taking any auxiliary data. In particular, we show how the phases of the Fourier components of a periodic structure can be fully recovered by deliberately choosing a probe wavelength of the diffracting radiation much smaller than the lattice constant of the structure. In the course of our demonstration, we accurately determine the slight asymmetry of the structure of nanocomposite phase gratings by light and neutron diffraction measurements.

1. Introduction

Diffraction experiments are usually a method of choice to determine the internal structure of bulk materials. Instead of a crystal, let us consider here the simple case of a planar one-dimensional phase grating, which is characterized by the spatial profile of the refractive index

$$\tilde{n}(x) = \sum_{s=-\infty}^{+\infty} \tilde{n}_s e^{\imath sGx}. \tag{1}$$

Here, G is the spatial frequency with $G = 2\pi/\Lambda$, where Λ is the grating spacing, and $|\tilde{n}_s| = n_s \in \mathbb{R}$ is the amplitude of the Fourier component at the index s. In the case of phase gratings ($\tilde{n}_{-s} = \tilde{n}_s^* \in \mathbb{C}$) the Fourier-series of the real-valued refractive index reads $n(x) = n_0 + 2\sum_{s=1}^{\infty} |\tilde{n}_s| \cos(sGx + \varphi_s)$, where $\varphi_s = \arg(\tilde{n}_s)$ is the relative phase of the Fourier component at the index s. By determining the Fourier components, i.e. amplitudes and phases of the Fourier components, the structure is fully retrieved. However, by measuring the intensities of diffracted signals – as it is usually done in standard diffraction experiments – only the magnitude of the s-th Fourier component that corresponds to the s-th diffraction order, can be obtained, whereas the phases φ_s are lost. The latter is sometimes called the phase problem of crystallography or diffraction (see, for instance, [1]). In principle, it can be overcome by measuring the phase differences between the wave incident to a sample of interest and each

#424233 https://doi.org/10.1364/OE.424233
Journal © 2021 Received 5 Mar 2021; revised 26 Apr 2021; accepted 27 Apr 2021; published 11 May 2021

Optics EXPRESS

diffracted wave interferometrically, which, however, is found to be utterly difficult in many relevant cases.

Sophisticated techniques have been developed to recover the phase information [1,2] either by so-called non-physical methods (direct methods, isomorphous replacement and anomalous scattering) or by introducing – sometimes demanding – experimental procedures to provide a physical solution [3–6]. Due to the importance of this problem that – as seen from a general point of view – remains unsolved to this day, discussions and suggestions of solutions for important particular cases have been provided for decades and are ongoing within the frame of many theoretical as well as some experimental studies (see, for instance, [7–17]). Surprisingly, sticking to traditional diffraction experiments combined with the well-known rigorous coupled-wave analysis (RCWA) [18] can indeed provide all necessary information in many cases if experimental settings are chosen carefully, as we will show here. In particular, we demonstrate by means of simple examples – one-dimensional, non-sinusoidal phase gratings – how such an approach to a solution to the phase problem of diffraction can be obtained with not more than the usual experimental effort in diffraction experiments. The technique is applicable to samples generating diffraction patterns for any type of radiation useful for structure determination (X-rays, electrons, laser light, and neutrons, for instance). We apply our approach to the problem of determining deviations of the periodic refractive index profiles of holographic nanoparticle-polymer composite (NPC) gratings [19] from their ideal sinusoidal form. NPCs consist of a photopolymer host that is uniformly dispersed with inorganic or organic nanoparticles having a large difference in refractive index between nanoparticles and the cured photopolymer. Because nanoparticles can be assembled under holographic exposure by means of the so-called "holographic assembly of nanoparticles in polymer" [20], this holographic assembling technique provides NPC volume gratings with very large refractive index modulation amplitudes (Δn), for example, as high as 0.045 and 0.030 at recording wavelengths of 532 and 640 nm [21,22], respectively, to be used as volume holographic diffractive elements in head-mounted displays for augmented/mixed reality. Other holographic applications of NPC gratings include holographic data storage, display technology and slow-neutron beam control [19,23–26]. The information on obtained grating profiles is also useful for our understanding of holographic formation processes in NPCs [27,28].

2. Statement of the problem

Holographic gratings were prepared from a photopolymerizable NPC material. As reported in the past [29], SiO_2 nanoparticles (with the average diameter of 13 nm and the bulk refractive index n_n of 1.46) dispersed in a solution of methyl isobutyl ketone are mixed with methacrylate monomers, 2-methyl-acrylic acid 2-4-[2-(2-methyl-acryloyloxy)-ethylsulfanylmethyl]-benzylsulfanyl-ethyl ester (the formed polymer refractive index n_p is 1.59 at 589 nm). The doping concentration of SiO_2 nanoparticles was 34 vol.%. Photoinitiator titanocene (Irgacure 784, Ciba) is also mixed in 1 wt.% with respect to the monomer to provide photosensitivity in the green. The above chemical mixture is cast on a glass plate. It is dried in an oven and finally covered with another glass plate, separated from the first one by spacers of known thickness. We employ a two-beam interference setup to write an unslanted transmission NPC grating by superposition of two mutually coherent s-polarized beams of equal light intensities from a diode-pumped frequency-doubled Nd:YVO_4 laser operating at 532 nm. Two NPC gratings were prepared: G1 at grating spacing Λ of 5 μm and with the thickness d of about 13 μm, and G2 at spacing Λ of 1 μm and with $d \approx 50\,\mu$m. In the bright regions of the interference pattern irradiating the sample, the photoinitiator triggers photopolymerization. Monomer is consumed there by the formation of polymer. Due to the resulting chemical potential gradient, a mutual diffusion process of unreacted monomer and nanoparticles sets in, leaving the dark regions enriched with nanoparticles [19]. It is important to note that, while the interference pattern is sinusoidal, the phase grating will be non-sinusoidal with nonzero higher Fourier components ($|s|>1$ in Eq. (1)) due to the interplay of nonlinear

Optics EXPRESS

processes governed by the photopolymerization-driven mutual diffusion process for the formation of spatial density modulations of the formed polymer and nanoparticles. (Such characteristic features of the nanoparticle density profile can also be assessed by various theoretical models [27,30].) Thus, however elaborate the described production process might be, it is subject to continuing optimization of material parameters and recording conditions which affect grating formation. Therefore, information as accurate as possible about the process outcome is desired, i.e. information about the redistribution of the nanoparticles dispersed in monomer under holographic exposure, which would eventually determine the exact form of the periodic refractive index profile given by Eq. (1). It is the latter we investigate by our proposed method here.

Figure 1 (a) shows an optical micrograph of G1 taken close to the maximum contrast position of the Talbot carpet [31–33], which can be observed for pure phase gratings using an optical microscope. It can be seen that SiO_2 nanoparticles (narrow, dark fringes, corresponding to lower refractive index regions) and the formed polymer (wide, bright fringes, corresponding to higher refractive index regions) are periodically arranged as a result of holographic assembly of nanoparticles [20]. Their distribution, shown in Fig. 1 (b), is not perfectly sinusoidal. In Fig. 1 (c), a section of a map of the optical path length difference of a sibling of G1 (also at $\Lambda = 5\ \mu$m) measured by digital holographic microscopy (DHM-R2100 by Lyncée Tec) is shown. The measurements were made with a 20X objective at a wavelength of $\lambda = 684.9$ nm. Also in this case, it is clearly seen from the sum of about 100 lines taken along the grooves of the optical path length difference map that the pattern is not purely sinusoidal, as shown in Fig. 1 (d). Thus, the Fourier series describing both distribution patterns and, therefore, the refractive index profiles must certainly include higher order Fourier terms, at $|s|>1$.

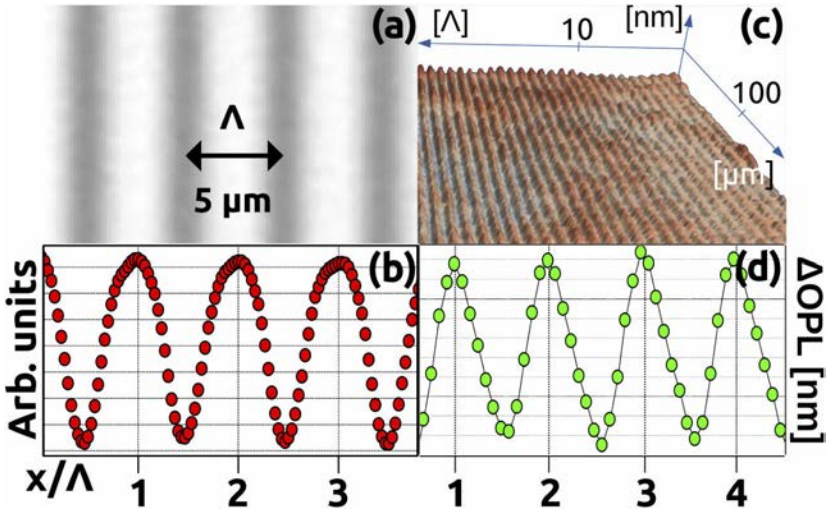

Fig. 1. (a) Optical micrograph of the holographic SiO_2 nanoparticle dispersed NPC grating G1 in transmission mode. (b) Sum of 100 lines of grayscale values of the micrograph in Fig. 1 (a). (c) Optical path length difference (ΔOPL, in units of nanometers; optical path length is defined as refractive index times distance) as a function of position on a grating similar to G1, measured by digital holographic microscopy. (d) Average over 100 lines in Fig. 1 (c). It is clearly seen that both profiles [(b) and (d)] exhibit higher order Fourier components.

Optics EXPRESS

3. Retrieval of the Fourier components' relative phases – experimental design and analysis

In many diffraction experiments aiming at structure determination, diffraction by a sample occurs in Bragg regime [34]: For optically thick samples and for relatively large Bragg angles, at most two waves propagate simultaneously and interfere within the sample at a given angle of incidence. One typically measures the dependence of the diffracted intensities upon the sample's rotation through angles of incidence Θ on a screen or a detector. In Bragg regime, peaks of the diffraction efficiency (DE, η) plotted versus Θ are relatively sharp and do not overlap as can be seen in Fig. 2 (a). Coupling (interference) of the two waves propagating within the sample's periodic structure (the refractive index modulation given by Eq. (1)) results in energy exchange between diffraction order pairs (the zero order beam and only one of the $\pm1, \pm2, \pm3, \ldots$ orders) as a function of Θ. The first Born approximation does not hold in such a case, but theories such as dynamical diffraction theory or Kogelnik's theory (see, for instance, [35,36]) can be deployed for modelling data taken in Bragg regime. However, the relative phases φ_s of Fourier components cannot be retrieved since multi-wave coupling of the corresponding waves does not occur at any Θ.

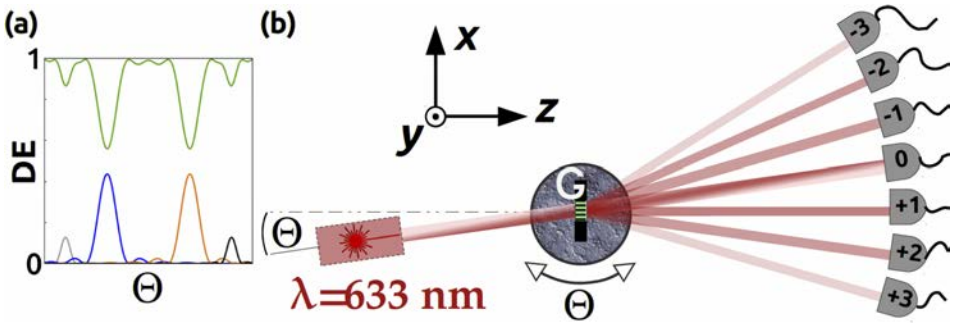

Fig. 2. (a) Plot of typical DE in the Bragg regime as a function of angle of incidence Θ. (b) Multi-wave coupling data of the grating G1 are obtained diffracting a He-Ne laser of a few mm beam width at a wavelength of $\lambda = 633$ nm, much shorter than the grating spacing of 5 μm. A grating is placed on a motorized stage which is rotated about the y-axis.

Now, in order to achieve such multi-wave coupling in diffraction and, thereby, to determine the relative phases φ_s of G1's structure, we apply visible light of wavelength $\lambda \ll \Lambda$ as a probe in our diffraction experiment, such that Λ is about an order of magnitude longer than the wavelength of the probe beam. By intentionally choosing λ much shorter than it would seem appropriate, we can leave the Bragg regime behind and allow for multi-wave coupling to occur within the periodic structure of the sample. From the Bragg equation $s\lambda = 2\Lambda_s \sin\Theta_s$ (Θ_s is the Bragg angle for the Fourier component at the index s) it is clear that the diffraction angle decreases with a decrease in λ, so that diffraction peaks of a given width overlap and the experiment can no longer be described in the Bragg regime. Clearly, more than just two waves propagate and interfere inside the sample at angles Θ for which observed peaks overlap considerably [see Fig. 2 (b)]. A rule of thumb on how to achieve multi-wave coupling can be derived by looking for parameter value combinations that provide for sufficient peak overlap of neighboring diffraction orders of considerable strength, which can be expressed as

$$\frac{\lambda d}{2n_0\Lambda^2} < 1. \tag{2}$$

Optics EXPRESS

The angular dependence data obtained by multi-wave coupling diffraction can be modelled by multiwave analysis theories such as the RCWA [18,37]. Here, the strategy is to solve Maxwell's equations in each of three regions (input, grating, output) such that the tangential components of the solutions of neighbouring regions match at these interfaces. Phase information of the Fourier components of the refractive index profile given by Eq. (1) is inherently included in the RCWA. A set of coupled-wave equations is solved by calculating eigenvalues and eigenvectors of a matrix directly related to those Fourier components. The amplitudes at arbitrary diffraction orders are found by employing the boundary conditions. In our work RCWA was used to fit the experimental DE defined as $\eta_s = I_s/I_{\mathrm{tot}}$, with the diffracted intensity I_s at the diffraction order s and the sum of all diffracted intensities behind the sample I_{tot}, and yield the amplitudes and phases of the corresponding Fourier components at the index s required to fully reconstruct $n(x)$.

4. Experimental results

To measure the angular dependence data, an s-polarized beam of a He-Ne laser ($\lambda = 633$ nm) was used to observe diffraction signals from G1 being rotated about the y-axis (perpendicular to the plane of incidence) at angles Θ ($-55° \ldots + 55°$), as is shown in Fig. 2 (b). Angular dependences of the diffracted intensities $I_s(\Theta)$ at $s = 0, \pm1, \pm2, \pm3$ were recorded by Si-photodiodes placed at the locations of the diffraction spots observed on a screen. The results are shown in Fig. 3. Due to the small ratio $\lambda/\Lambda \approx 0.1$ in our experiment, the Bragg angles $\Theta_s = \pm 3.6°, \pm 7.3°, \pm 10.9°$ at $s = \pm1, \pm2, \pm3$, respectively, are small, too. All seven observable diffraction orders overlapped within $\pm20°$ and exhibited sufficiently large DE to be readily detected. Solid curves in Fig. 3 are least-squares fits to the RCWA. Fitting was performed including all data points. The RCWA is in excellent agreement with the experimental data, by which we can achieve accurate structure determination as is shown below: Estimations for the amplitudes $|n_1|, |n_2|$ and $|n_3|$ of the Fourier components as well as their phases φ_2 and φ_3 as obtained by the RCWA fit are given in the second column of Table 1.

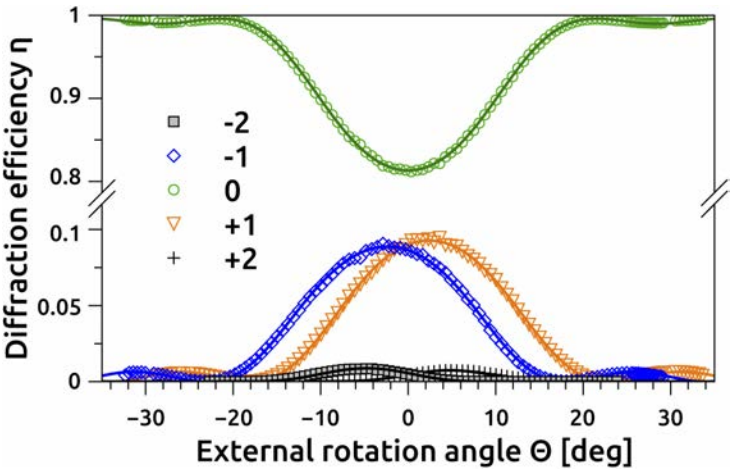

Fig. 3. Measured angular dependence (data points) of the DE for the $\pm2, \pm1, 0$ orders for G1 at a wavelength of 633 nm. Error bars are much smaller than the symbols. The ±3 orders were measured and included in the fitting procedure, but their DE is small and not shown here. Solid curves are RCWA fits to the data at seven diffraction orders, yielding φ_2 and φ_3 (see Table 1).

The values of φ_2 and φ_3 were – without loss of generality – obtained with respect to φ_1 set to zero. The spatial refractive index profile as calculated from fit parameter estimations is shown in

Optics EXPRESS

Table 1. Amplitudes and relative phases for the Fourier coefficients of refractive index profiles for G1 and G2. The values were determined by RCWA fits to the data with φ_1 set to zero (see text). Resulting profiles obtained from light and neutron diffraction measurements are shown in Figs. 4 and 6, respectively.

Grating:	G1	G2
Parameters:	$\Lambda = 5\,\mu$m, $d \approx 13\,\mu$m	$\Lambda = 1\,\mu$m, $d \approx 50\,\mu$m
Probe beam:	light @ $\lambda = 633$ nm	neutrons @ $\lambda = 1.7$ nm
$\lvert n_1 \rvert$	$4.9382(37) \times 10^{-3}$	$2.592(28) \times 10^{-6}$
$\lvert n_2 \rvert$	$1.072(15) \times 10^{-3}$	$5.03(58) \times 10^{-7}$
$\lvert n_3 \rvert$	$1.72(48) \times 10^{-4}$	n. a.
φ_1	$:= 0$	$:= 0$
φ_2	$1.0581(39)\pi$	$0.995(27)\pi$
φ_3	$0.37(15)\pi$	n. a.

Fig. 4 (solid, black curve). Since the refractive index modulation amplitude of a recorded NPC grating is proportional to $n_n - n_p$ [38], the SiO_2 rich regions correspond to the low refractive index regions. Comparison with the data of Fig. 1 (b) (filled, red circles in Fig. 4) makes the qualitative agreement obvious, thereby demonstrating the validity of our approach. Even the slight asymmetry in the profile (slight flattening on the left side of each peak), which may be caused by spatially nonuniform lateral shrinkage during holographic exposure, is captured by the RCWA analysis of the diffraction data as can be seen from the inset in Fig. 4.

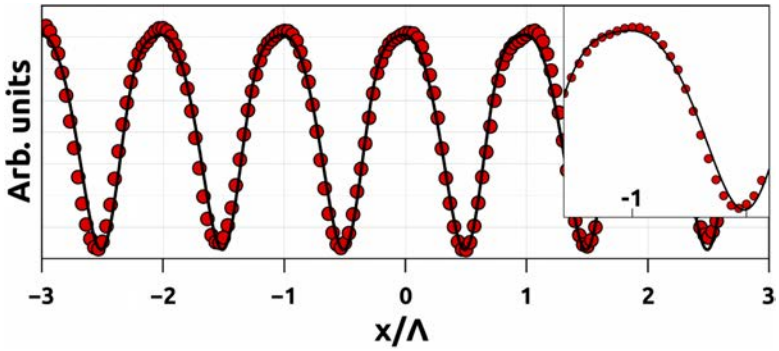

Fig. 4. Plotted are the data points (filled, red circles) extracted from the grayscale image in Fig. 1(a) [as shown in Fig. 1 (b)]. The refractive index profile of G1 obtained from the RCWA fit-parameter estimation (as given in Table 1) was rescaled and shifted (solid, black curve) for direct comparison to the data points in the present plot. Peaks correspond to the polymer ridges of the structure. Inset: Third peak from the left, magnified. Even detailed features of the micrograph data are reproduced, as shown in the inset.

Next, the refractive index profile of G2 ($\Lambda = 1\,\mu$m, $d \approx 50\,\mu$m) is to be retrieved. Accurately resolving such structures by an optical microscope is possible but not straightforward, which underlines the potential impact of our solution to the phase problem, especially for refractive index profiles, which have structural dimensions of the order of light wavelengths. In the case of G2, Kogelnik's theory [36] allows to roughly estimate the expected peak width (the angular distance between the minima adjacent to the Bragg angle Θ_1 at $s = 1$ in an angular dependence plot of DE) as $2n_0\Lambda/d \approx 3.4°$. For wavelengths around the higher and lower limits of the visible range, one expects $\Theta_1 \approx 17°$ at $\lambda = 633$ nm and $\Theta_1 \approx 10°$ at a UV wavelength of $\lambda = 351$ nm. Thus, it is difficult to produce peak overlap to transfer the diffraction process from the Bragg

Optics EXPRESS

regime to the multi-wave coupling regime for the determination of the refractive index profile of G2, by use of table-top laser light sources. However, a key point of our approach is that depending on the particular material class investigated, there might be other kinds of radiation available for diffraction experiments to obtain data similar to the ones shown in Fig. 3. For instance, since the refractive index profile is produced by the density modulation of one of the involved material components (nanoparticles, in our case), it is known that small angle neutron scattering (SANS; see, for instance, [39]) provide well-established tools [40]: For a typical de Broglie wavelength of neutrons in a SANS experiment of 1 nm, say, one may expect Bragg angles $\Theta_1 \approx \lambda/(2\Lambda)$ of the order of 0.03°, which can be detected with state-of-the-art SANS instruments, thanks to long sample-detector distances (up to 20 m) and sufficient spatial resolution of detectors. Thus, considerable peak-overlap for G2 and, therefore, multi-wave coupling is achievable with neutrons.

The neutron experiment was performed by use of the instrument SANS-I of the SINQ neutron source of Paul-Scherrer Institute in Villigen, Switzerland. Cold neutrons at a mean wavelength of 1.7 nm (width of wavelength distribution $\Delta\lambda/\lambda \approx 10\%$) were diffracted from G2. The beam divergence was limited to about 1 mrad, using collimation slits. The diffracted intensities were measured using a two-dimensional detector of $7.5 \times 7.5\,\mathrm{mm}^2$ pixel size. To adjust the peak width (estimated by $2\Lambda/d$, see our above discussion) and the peak height for our purpose, G2 was tilted around its grating vector by $\zeta \approx 60°$ which increases the effective thickness to $d \rightarrow d/\cos\zeta$, i. e. by a factor of two [40,41]. The results are shown in Fig. 5. Similarly to the DE of G1 shown in Fig. 3, the observed diffraction took place in the multi-wave coupling regime, that is, many (five, in this case) diffraction orders are observable within the angular range of $\Theta = \pm 0.25°$. Applying the RCWA fit, we were, again, able to extract the full information (amplitudes *and* phases) of the grating's Fourier components up to the 2nd-order. They are given in Table 1 (third column). Simulations of the DE assuming $\varphi_2 = 0$ instead of the experimentally obtained value are also plotted (red, dashed curves) in Fig. 5. The disagreement of simulation at $\varphi_2 = 0$ and data is easily resolved in a standard SANS experiment. The neutron-refractive index profile of G2 – corresponding to the spatial density distribution of formed polymer and nanoparticles – as calculated from the RCWA parameter estimation is shown in Fig. 6 together with its counterpart, assuming $\varphi_2 = 0$, for comparison. Note that the refractive index modulation amplitude for neutrons is proportional to $-(b_n\rho_n - b_p\rho_p)$, where b_n (b_p) and ρ_n (ρ_p) are the mean bound coherent scattering length [39] and the atomic density of nanoparticles (the formed polymer), respectively. Since $b_n\rho_n$ is larger than $b_p\rho_p$ for SiO_2 nanoparticles [40], the SiO_2 rich regions correspond to lower refractive index regions in Fig. 6, as similar to Fig. 4. No third order component was measurable for G2 and therefore the profile in Fig. 6 is symmetric, in contrast to the profile of G1. We attribute this difference to the mutual diffusion process, which is much more significant in G2 due to the smaller grating spacing.

For the data analysis procedure, the RCWA formulation as published in Ref. [18] was implemented in home-made python code. With RCWA, Maxwell's equations are solved in entrance-, grating-, and exit-regions, with the proper boundary conditions applied. In this particular formulation [18], a solution of the corresponding diffraction problem formulated as an eigenstate problem is found. The eigenvalues and eigenvectors are then inserted in the space harmonics of the fields' exponentials. The numerical stability criteria – energy conservation and convergence – are discussed in detail in Ref. [18]. Failure of convergence is avoided by appropriate normalization for yielding only negative exponents. Numerical efficiency is supported by eliminating the amplitudes of the forward and backward diffracted fields, and solving a set of linear equations to obtain the coefficients according to the boundary conditions. The coefficients are, then, used to retrieve the amplitudes of the diffracted fields. For fitting the light-optical and neutron-optical diffraction data in the RCWA expansion, 7 modes $(\pm 3, \pm 2, \pm 1, 0)$ and 5 modes $(\pm 2, \pm 1, 0)$ were considered, respectively. To find the eigenvalues and eigenvectors the linalg.eig python library (for complex matrices) was used. The target function of the fitting procedure is

Optics EXPRESS

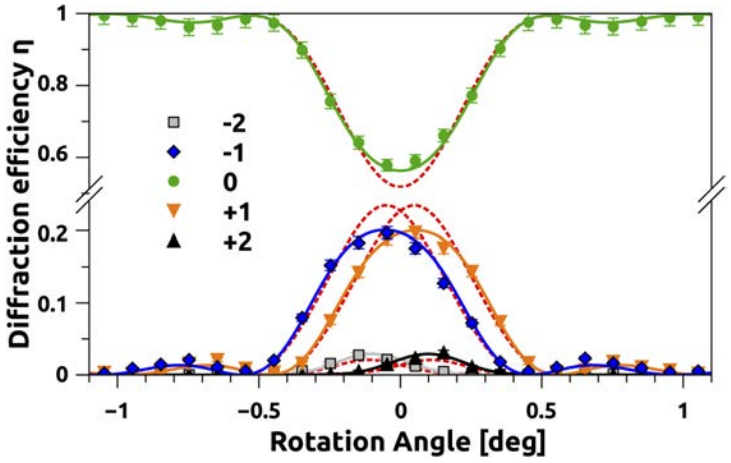

Fig. 5. Measured angular dependence (data points) of DE for G2 at the $\pm 2, \pm 1, 0$ orders and at the neutron wavelength of 1.7 nm. Five-wave coupling was observed near the normal incidence. An RCWA fit (solid curves) again allows to retrieve amplitudes and phases of the grating's Fourier components. The resulting fit parameter estimation is given in Table 1. To illustrate the importance of the correct phase value, simulations for $\varphi_2 = 0$ (dashed, red curves) instead of the experimentally obtained value $\varphi_2 = 0.995\,\pi$ are added.

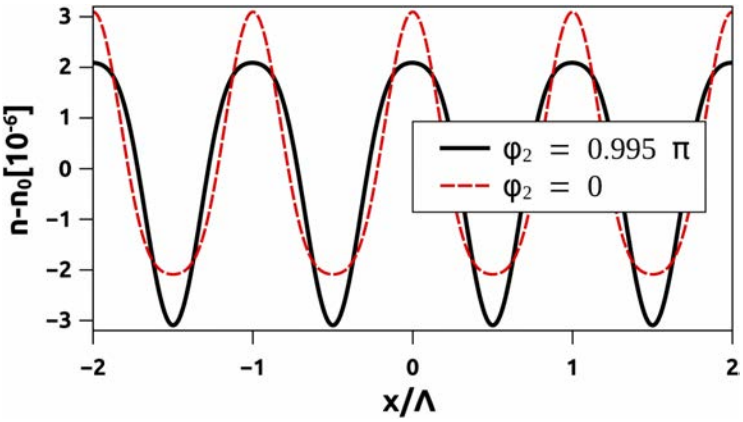

Fig. 6. The neutron-refractive index profile of G2 calculated from the RCWA fit-parameter estimation as given in Table 1 (solid, black curve). The neutron-refractive index profile of G2 is also plotted for $\varphi_2 = 0$ (dashed, red curve) instead of the experimentally obtained value $\varphi_2 = 0.995\,\pi$.

written as weighted least-squares function $\sum_j[(\eta_j - f_j(pars)/\Delta\eta_j]^2$, which was minimized using the python scipy.optimize.leastsq solver. Here, η_j is the experimentally measured value of the diffraction efficiency at position j, f_j is the value of the model function (solution of the RCWA) at position j, "*pars*" refers to the free fitting parameters and $\Delta\eta_j$ is the experimental error of the data point at position j. The free fitting parameters were the refractive index modulations n_1, n_2, and n_3 and the relative phases φ_2 and φ_3 as well as the grating thickness d. Approximate initial values for the parameters were estimated by manually and iteratively adjusting RCWA simulations with reasonable values from our previous works. The initial phases were chosen near

Optics EXPRESS

zero or π, which is what is expected for holographic gratings. Our a priori knowledge is that our holographic gratings are periodic, are pure phase gratings, i.e., $n_s \in \mathbb{R}$ (no absorption grating), and that a relatively small number of modes (7 and 5 for light- and neutron-data, respectively) is sufficient to predict the refractive index profiles. These conditions are well justified for our holographically recorded NPC gratings. They might not hold for gratings deliberately designed to, e. g., suppress particular higher diffraction orders. No loss terms were introduced. As we employed a TE polarized probe beam and in-plane (not conical, see Fig. 2) geometry, the RCWA calculation was stable and converged fast [18,37,42]. Using a standard laptop with a CPU at 1.7GHz clock speed, the time for minimizing the target function for a data set of 625 data points was about 26 hours (light diffraction data set, 7-wave-coupling). Fitting curves using the resulting fit parameter estimations were obtained within a few seconds.

5. Discussion

In a nutshell, which conditions need to be fulfilled for our approach to work for a given sample? *(i)* The sample structure must be periodic, the period known approximately. *(ii)* A suitable probe radiation that interacts sufficiently with the structure and provides for inequality Eq. (2) to be fulfilled must be available for carrying out experiments in the multi-wave coupling diffraction regime. *(iii)* Detection of potentially weaker higher diffraction orders must be guaranteed for the considered probe radiation, depending on the desired resolution of refractive index profile features.

The RCWA formulation in Ref. [18] applied to our case implied only low-dimensional matrices (7×7 for light, 5×5 for neutrons). It yielded excellent results needing only direct solvers (i.e. non-iterative solvers). For our holographically prepared phase gratings, smooth refractive-index profiles are expected, the material is not conducting and, thus, the used RCWA formulation [18] is converging fast for TE polarization. We tested the stability of the results of our optimization procedure by variation of the initial values for the phases φ_2 and φ_3. For instance, initial values for φ_2 and φ_3 both near zero or both near π were introduced. In any case, the resulting fitting parameter estimations converged to values as given in Table 1. We would like to emphasize that the method itself contains the full complex refractive index and thus the imaginary part of the Fourier-coefficients can be readily implemented. Therefore, our approach can be used for absorption gratings as well and also for mixed gratings. It is not limited to the analysis of pure phase gratings.

Of course, it is – in many cases – more convenient to apply optical microscopy for the estimation of the refractive index profile, but resolution limits of microscopy are laborious to overcome in the range of typical structure constants of several hundred nanometers. Furthermore, electron microscopy and physico-chemical analyses often depend on sample preparation techniques – producing thin slices or breaking samples to look at surfaces – that are cumbersome or even unreliable in the sense that they could, in the worst case, mechanically alter the structure to be investigated. Our damage-free technique, however, can provide sufficient resolution in bulk so long as a suitable state-of-the-art instrument, meeting the wavelength requirements to work in multi-wave coupling regime for a structure of interest, can be accessed at one of the many facilities worldwide. Resolution is limited by the – usually excellent – detector sensitivity and background suppression necessary for reliable observation of weak higher-order diffraction signals. The RCWA analysis carried out here on an off-the-shelf PC can be applied to more complicated structures by using more powerful computation infrastructure, nowadays available at many institutions.

Finally, we note that the technique presented here is closely related to previous proposals to employ multi-wave coupling (see, for instance, [2–5]). The fundamental difference between those and our approach is, however, that apart from a careful choice of wavelengths, only standard

Optics EXPRESS

diffraction procedures are applied here. No extra data needs to be taken. Our approach can be seen as generalization of what is discussed in the recent Ref. [16].

6. Conclusion

In summary, we have demonstrated the determination of refractive index profiles by diffraction from one-dimensional holographic phase gratings recorded in SiO_2 nanoparticle-dispersed NPC films. We have shown that full phase retrieval can be made without the need for extra data collection schemes. In particular, by choosing the probe wavelength some orders of magnitude shorter than the structural dimensions being investigated, Bragg regime diffraction can be turned into diffraction in the regime of multi-wave coupling for any given sample combined with a suitable type of probe radiation (X-rays, electrons, visible light, and neutrons, for instance). Fitting of a multi-wave coupling model such as the well-known RCWA (valid in the multi-wave coupling regime) to the resulting angular dependence data allows for the accurate determination not only of amplitudes but also of phases of the Fourier components of generic profiles of refractive index modulation. Such information is useful for investigation of grating-formation mechanisms and optimization of nanocomposite gratings. When dealing with photonic structures (like gratings) it is a common practice to avoid multi-wave coupling for ease of the analysis, in particular when it comes to the evaluation of the underlying parameters. Here, we have shown that getting rid of this habit and embracing the usually shunned multi-wave coupling regime can pay off at the prize of a relatively low increase in experimental and analytical complication.

Funding. Ministry of Education, Culture, Sports, Science and Technology (15H03576, 25-03052).

Acknowledgements. We would like to thank G. Heuberger for preliminary experimental work. Open access funding provided by University of Vienna.

Disclosures. The authors declare no conflicts of interest.

Data availability. Data underlying the results presented in this paper are not publicly available at this time but may be obtained from the authors upon reasonable request.

References

1. H. A. Hauptman, "The phase problem of x-ray crystallography," Rep. Prog. Phys. **54**(11), 1427–1454 (1991).
2. M. Woolfson and H.-F. Fan, *Physical and non-physical methods of solving crystal structures* (Cambridge University, 1995).
3. L. D. Chapman, D. R. Yoder, and R. Colella, "Virtual bragg scattering: A practical solution to the phase problem in diffraction," Phys. Rev. Lett. **46**(24), 1578–1581 (1981).
4. S.-L. Chang, "Direct determination of x-ray reflection phases," Phys. Rev. Lett. **48**(3), 163–166 (1982).
5. Q. Shen, "Solving the phase problem using reference-beam x-ray diffraction," Phys. Rev. Lett. **80**(15), 3268–3271 (1998).
6. E. Wolf, "Solution of the phase problem in the theory of structure determination of crystals from x-ray diffraction experiments," Phys. Rev. Lett. **103**(7), 075501 (2009).
7. A. Roger and D. Maystre, "Inverse scattering method in electromagnetic optics: Application to diffraction gratings," J. Opt. Soc. Am. **70**(12), 1483–1495 (1980).
8. G. J. Kleywegt, "Validation of protein crystal structures," Acta Crystallogr. D **56**(3), 249–265 (2000).
9. A. Rathsfeld, G. C. Hsiao, and J. Elschner, "Grating profile reconstruction based on finite elements and optimization techniques," SIAM J. Appl. Math. **64**(2), 525–545 (2004).
10. G. Bao, P. Li, and H. Wu, "A computational inverse diffraction grating problem," J. Opt. Soc. Am. A **29**(4), 394–399 (2012).
11. R. Horstmeyer, J. Chung, X. Ou, G. Zheng, and C. Yang, "Diffraction tomography with fourier ptychography," Optica **3**(8), 827–835 (2016).
12. L. Liberman, Y. Israel, E. Poem, and Y. Silberberg, "Quantum enhanced phase retrieval," Optica **3**(2), 193–199 (2016).
13. R. P. Millane, "The phase problem for one-dimensional crystals," Acta Crystallogr., Sect. A: Found. Adv. **73**(2), 140–150 (2017).
14. M. Fally, J. Klepp, M. A. Ellabban, H. Eckerlebe, P. K. Pranzas, J. Guo, and Y. Tomita, "Retrieving the refractive index profile of a holographic grating by diffraction experiments," Proc. SPIE **11030**, 110300I (2019).
15. J. J. Donatelli and J. C. H. Spence, "Inversion of many-beam bragg intensities for phasing by iterated projections: Removal of multiple scattering artifacts from diffraction data," Phys. Rev. Lett. **125**(6), 065502 (2020).

Optics EXPRESS

16. B. Heacock, D. Sarenac, D. G. Cory, M. G. Huber, J. P. W. MacLean, H. Miao, H. Wen, and D. A. Pushin, "Neutron sub-micrometre tomography from scattering data," IUCrJ **7**(5), 893–900 (2020).
17. M. Chen, D. Ren, H.-Y. Liu, S. Chowdhury, and L. Waller, "Multi-layer born multiple-scattering model for 3d phase microscopy," Optica **7**(5), 394–403 (2020).
18. M. G. Moharam, E. B. Grann, D. A. Pommet, and T. K. Gaylord, "Formulation for stable and efficient implementation of the rigorous coupled-wave analysis of binary gratings," J. Opt. Soc. Am. A **12**(5), 1068–1076 (1995).
19. Y. Tomita, E. Hata, K. Momose, S. Takayama, X. Liu, K. Chikama, J. Klepp, C. Pruner, and M. Fally, "Photopolymerizable nanocomposite photonic materials and their holographic applications in light and neutron optics," J. Mod. Opt. **63**(sup3), S1–S31 (2016).
20. Y. Tomita, N. Suzuki, and K. Chikama, "Holographic manipulation of nanoparticle distribution morphology in nanoparticle-dispersed photopolymers," Opt. Lett. **30**(8), 839–841 (2005).
21. Y. Tomita, T. Aoi, S. Hasegawa, F. Xia, Y. Wang, and J. Oshima, "Very high contrast volume holographic gratings recorded in photopolymerizable nanocomposite materials," Opt. Express **28**(19), 28366–28382 (2020).
22. A. Narita, J. Oshima, Y. Iso, S. Hasegawa, and Y. Tomita, "Red-sensitive organic nanoparticle-polymer composite materials for volume holographic gratings with large refractive index modulation amplitudes," Opt. Mater. Express **11**(3), 614–628 (2021).
23. Y. Ohe, M. Kume, Y. Demachi, T. Taguchi, and K. Ichimura, "Application of a novel photopolymer to a holographic head-up display," Polym. Adv. Technol. **10**(9), 544–553 (1999).
24. H. J. Coufal, D. Psaltis, and G. T. Sincerbox, eds., *Holographic Data Storage* (Springer-Verlag, 2000).
25. G. P. Crawford, "Electrically switchable bragg gratings," Opt. Photonics News **14**(4), 54–59 (2003).
26. J. W. An, D. D. Do, N. Kim, and K. Y. Lee, "Expansion of channel number in optical demultiplexer using cascaded photopolymer volume gratings," IEEE Photonics Technol. Lett. **18**(6), 788–790 (2006).
27. Y. Tomita, N. Suzuki, K. Furushima, and Y. Endoh, "Volume holographic recording based on mass transport of nanoparticles doped in methacrylate photopolymers," Proc. SPIE **5939**, 593909 (2005).
28. K. Chikama, K. Mastubara, S. Oyama, and Y. Tomita, "Three-dimensional confocal raman imaging of volume holograms formed in ZrO_2 nanoparticle-photopolymer composite materials," J. Appl. Phys. **103**(11), 113108 (2008).
29. N. Suzuki and Y. Tomita, "Silica-nanoparticle-dispersed methacrylate photopolymers with net diffraction efficiency near 100 %," Appl. Opt. **43**(10), 2125–2129 (2004).
30. G. Karpov, V. Obukhovsky, T. Smirnova, and V. Lemeshko, "Spatial transfer of matter as a method of holographic recording in photoformers," Opt. Commun. **174**(5-6), 391–404 (2000).
31. J. W. Goodman, *Introduction to Fourier Optics* (W. H. Freeman and Company, 2017).
32. P. Zhou and J. H. Burge, "Analysis of wavefront propagation using the talbot effect," Appl. Opt. **49**(28), 5351–5359 (2010).
33. J. Wen, Y. Zhang, and M. Xiao, "The Talbot effect: recent advances in classical optics, nonlinear optics, and quantum optics," Adv. Opt. Photonics **5**(1), 83–130 (2013).
34. M. Moharam, T. Gaylord, and R. Magnusson, "Criteria for Bragg regime diffraction by phase gratings," Opt. Commun. **32**(1), 14–18 (1980).
35. B. W. Batterman and H. Cole, "Dynamical diffraction of X rays by perfect crystals," Rev. Mod. Phys. **36**(3), 681–717 (1964).
36. H. Kogelnik, "Coupled wave theory for thick hologram gratings," Bell Syst. Tech. J. **48**(9), 2909–2947 (1969).
37. E. Popov, ed., *Gratings: Theory and Numeric Applications* (Universitaire de Provence, 2014).
38. N. Suzuki, Y. Tomita, and T. Kojima, "Holographic recording in TiO_2 nanoparticle-dispersed methacrylate photopolymer films," Appl. Phys. Lett. **81**(22), 4121–4123 (2002).
39. B. T. M. Willis and C. J. Carlile, *Experimental Neutron Scattering* (Oxford University, 2009).
40. M. Fally, J. Klepp, Y. Tomita, T. Nakamura, C. Pruner, M. A. Ellabban, R. A. Rupp, M. Bichler, I. Drevenšek-Olenik, J. Kohlbrecher, H. Eckerlebe, H. Lemmel, and H. Rauch, "Neutron optical beam splitter from holographically structured nanoparticle-polymer composites," Phys. Rev. Lett. **105**(12), 123904 (2010).
41. V. A. Somenkov, S. S. Shilstein, N. E. Belova, and K. Utemisov, "Observation of dynamical oscillations for neutron scattering by ge crystals using the inclination method," Solid State Commun. **25**(8), 593–595 (1978).
42. L. Li, "Use of fourier series in the analysis of discontinuous periodic structures," J. Opt. Soc. Am. A **13**(9), 1870–1876 (1996).